Journal of the Meteorological Society of Japan, Vol. 87, No. 5, pp. 913–921, 2009.
DOI:10.2151/jmsj.87.913

NOTES AND CORRESPONDENCE

On Forcing the Winter Polar Warmings in the Martian Middle Atmosphere during Dust Storms

Takeshi KURODA

Max Planck Institute for Solar System Research, Katlenburg-Lindau, Germany
Institute of Space and Astronautical Science, Japan Aerospace Exploration Agency, Sagamihara, Japan

Alexander S. MEDVEDEV, Paul HARTOGH

Max Planck Institute for Solar System Research, Katlenburg-Lindau, Germany

and

Masaaki TAKAHASHI

Center for Climate System Research, University of Tokyo, Kashiwa, Japan

(Manuscript received 25 March 2009, in final form 19 July 2009)

Abstract

Using a Martian general circulation model, we investigated the changes in the meridional circulation during planet-encircling dust storms on Mars that produce strong temperature vertical inversions in the middle atmosphere over winter polar regions. It is shown that vigorous poleward and downward transport, and, consequently, the adiabatic heating are caused by dissipating thermal tides, planetary and resolved small-scale gravity waves and eddies in almost equal degree. The increase of tidal forcing is mainly due to a stronger excitation in the summer hemisphere. Contribution of the stationary planetary wave (SPW) with the zonal wavenumber $s = 1$ increases during dust storms due to intensified generation in the lower atmosphere as well as due to more favorable vertical propagation. SPW ($s = 2$) varies less with the dust load, dissipates lower, and contributes to the warming only below ~ 0.1 mb. Transient planetary wave ($s = 1$, period ~ 5 sols) with a barotropic/baroclinic vertical structure provides up to 1/3 of the forcing by SPW ($s = 1$). For the first time, we demonstrated a significance of small-scale gravity waves and eddies in maintaining the meridional circulation in Martian middle atmosphere, at least in high winter latitudes during dust storms.

1. Introduction

Martian atmospheric temperatures, which are considerably warmer than would be expected from radiative equilibrium calculations, were numerously observed over the winter poles on Mars between 30 and 80 km (e.g., Deming et al. 1986; Theodore et al. 1993). Recently, a warming in the Martian thermosphere (between 100 and 130 km) was detected in high latitudes near the winter solstices (Keating et al. 2003; McCleese et al. 2008). It was recognized that these phenomena in both the middle atmosphere and thermosphere are induced by adiabatic heating (e.g., Barnes and Haberle 1996; Wilson 1997; Bougher et al. 2006; Medvedev and Hartogh

Corresponding author: Takeshi Kuroda, Max Planck Institute for Solar System Research, Max-Planck-Str. 2, Katlenburg-Lindau, 37191, Germany.
E-mail: kuroda@mps.mpg.de

2007). They arise due to a convergence of the meridionally transported air, and the associated downwelling over winter polar regions. In this paper, we consider the warmings in the middle atmosphere.

Viking Infrared Thermal Mapping instrument (IRTM) observations pointed out to a correlation between dust storms and temperature increases over the winter pole (Jakoski and Martin 1987). The dust storm occurred around the northern winter solstice (so-called 1977b storm) produced a strong polar warming. Wilson (1997) realistically reproduced this warming event with a general circulation model (GCM), while Forget et al. (1999) showed that a high opacity state can lead to a warm pole in the solstitial season in GCM simulations. These studies related the temperature enhancements at 30–80 km to the extension of the Hadley circulation cell into high latitudes. Several mechanisms can be responsible for such extensions. First, atmospheric dust lifted up from the surface intensifies the absorption of solar radiation, thus increasing the diabatic heating by tens K sol^{-1}. If the meridional circulation is consistent with a thermally driven nearly inviscid Hadley cell (Schneider 1977, 1983), the enhanced latitudinal gradient of radiative heating amplifies the meridional transport. In this case, the global thermal gradient rather than the local one is responsible for the poleward extension of the circulation cell, because the insolation is small in high winter latitudes. Second, the upward propagating planetary stationary waves (SPWs) can enhance Martian polar warmings, as discussed in Barnes and Hollingsworth (1987) using a quasi-geostrophic model. On the other hand, the importance of large-scale zonally asymmetric eddies (planetary waves and tides) has been discussed in the recent studies with GCMs. Wilson and Hamilton (1996) and Wilson (1997) pointed out that eddies possibly allow the meridional circulation to further extend to winter pole, thus causing the polar warmings. Medvedev and Hartogh (2007) argued that large-scale eddies are the primary drivers of the inter-hemispheric solstitial circulation, at least above 40 km.

Despite the recent advances in understanding the dust-induced warmings, many quantitative details remain unclear. What is a relative importance of thermal and mechanical forcings of the Hadley circulation? How do different types of eddies contribute to it? How does the radiative heating increased by airborne aerosol modify the waves? We address these and related issues in this paper with numerical simulations using a Martian GCM.

2. Model

We applied the Martian general circulation model (MGCM) (Kuroda et al. 2005), which was developed from the CCSR/NIES/FRCGC (Center for Climate System Research/National Institute of Environmental Studies/Frontier Research Center for Global Change, Japan) terrestrial GCM (Numaguti et al. 1995). It utilizes a spectral solver for the three-dimensional primitive equations, and has a comprehensive suite of physical parameterizations for the Martian atmosphere (Kuroda et al. 2005). The radiation scheme computes heating and cooling rates due to the absorption and emission by CO_2 infrared bands (under the local thermodynamic equilibrium), and by the atmospheric dust in both solar and infrared wavelengths between 0.2 and 200 μm. On the surface, the model uses the realistic topography, albedo and thermal inertia distributions. CO_2 condensation/sublimation scheme accounts for the change of air mass and the surface CO_2 snow cover. The model has been extensively validated against the existing measurements on Mars including the zonal mean climatology (Kuroda et al. 2005), baroclinic planetary waves (Kuroda et al. 2007), zonal-mean variability in mid- and high-latitudes (Yamashita et al. 2007), and the semiannual oscillations in tropics (Kuroda et al. 2008). All the experiments to be presented were carried out with 30 vertical σ-levels with the model lid at $\sim$ 80 km, and with T21 horizontal resolution (grid interval of $\sim 5.6^\circ$ in both longitude and latitude).

3. Results

For this study, a horizontally uniform total optical depth in the visible wavelengths $\tau = 0.5$ was specified for the "low dust" scenario, and $\tau = 3.0$ for the planet-encircling dust storm ("strong dust" scenario). The former quantity lies well within the dust opacities observed during "quiet" periods, and the latter value corresponds to a very strong dust storm (Smith 2004). Therefore, the simulated fields should be representative of the Martian atmosphere at "low dust" and "dusty" conditions. The vertical distribution of the aerosol mixing ratio was prescribed as $Q = Q_0 \exp\{0.01[1 - (p_0/p)]\}$, where Q_0, p_0 and p are the reference dust mixing ratio (that depends on the optical depth, e.g., 6.2 ppm of mass for $\tau = 1.0$), pressures at the reference (600 Pa) and

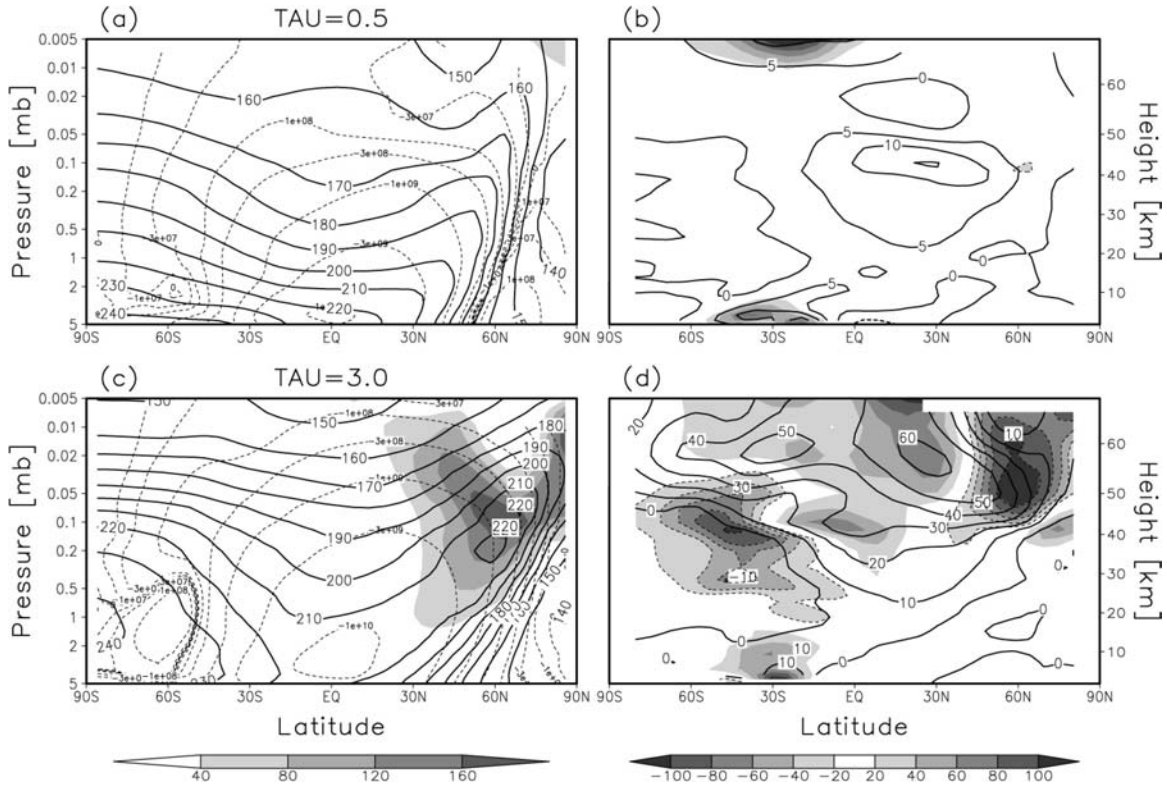

Fig. 1. Results of simulations for the "low dust" ($\tau = 0.5$) run (upper panels), and the "strong dust" ($\tau = 3.0$) (lower panels): (a) and (c) The zonal-mean temperature [K] (solid lines), meridional mass stream function [kg s^{-1}] (dashed lines, positive values denote counterclockwise circulation), and adiabatic heating rate [K sol^{-1}] (shades). (b) and (d) The residual meridional velocities $\bar{v}^*$ [m s^{-1}] (contours) and EP flux divergence $\nabla \cdot \mathbf{F}$ [m s^{-1} sol^{-1}] (shaded, negative values are surrounded by thin dashed lines).

any given level, respectively. This formula is a simplified version of the representation commonly used in Martian GCMs (Forget et al. 1999; Hartogh et al. 2005). It corresponds to a roughly uniform mixing ratio up to ~ 35 km, and to strong decays above. Both simulations started at $L_s = 180°$, and the results to be presented are the 20-day averaged fields near the Northern winter $L_s = 270°$.

As seen from Figs. 1a, c, the atmospheric thermal structure (solid lines) at $\tau = 3.0$ has significantly changed compared to the "low dust" simulation. The zonal mean temperature increased in the southern (summer) hemisphere below ~ 0.01 mb due to a stronger absorption of solar radiation by dust as well as in the high latitude northern (winter) hemisphere where the direct diabatic heating by aerosol plays little role. Instead, the enhanced adiabatic heating (shown in shades in Figs. 1a, c) is mainly responsible for 40–60 K warmer winter polar air in the middle atmosphere. This adiabatic heating, $\bar{q}_{ad} = -R\overline{w}^*\overline{T}/c_pH$, where $\overline{w}^*$ is the vertical residual velocity, overbars denote zonal averaging, R is the gas constant, T is the temperature, c_p is the heat capacity, and H is the density scale height, is associated with the downward branch of the meridional transport cell. The mass stream functions are shown with dashed lines in Figs. 1a, c. In both simulations the cell with rising motions approximately over the southern midlatitudes, the descending air over the North Pole, and a northward transport between the rising and descending points in the middle atmosphere, dominate. The corresponding residual meridional velocities, $\bar{v}^*$, are plotted in Figs. 1b, d. It is seen that in the "low dust" simulation (Figs. 1a, b), the circulation cell closes down near the model lid in the southern hemisphere mainly due to the presence of the Rayleigh friction sponge layer above 0.01 mb. The maximum of $\bar{v}^*$ (~ 15 m s^{-1}) occurs in the northern hemisphere around ~ 0.1 mb. During the

global dust storm (Figs. 1c, d), the circulation closes lower down in the southern hemisphere, and the meridional velocity $\bar{v}^*$ increases ~ 4 times (up to ~ 70 m s^{-1}). The gray-scale shades denote the divergence of the Eliassen-Palm (EP) fluxes, $\nabla \cdot \mathbf{F}$. Here $\mathbf{F} = (0, \cos\phi[\bar{u}_z \overline{v'\theta'}\bar{\theta}_z^{-1} - \overline{v'u'}], \cos\phi\{[f - (\bar{u}\cos\phi)_y]\overline{v'\theta'}\bar{\theta}_z^{-1} - \overline{w'u'}\})$, ϕ is the latitude, u is the zonal wind velocity, θ is the potential temperature, primes denote deviations from the zonal-mean values, and f is the Coriolis parameter. It follows from the mean zonal momentum equation in the transformed Eulerian mean formulation (Andrews and McIntyre 1976; Andrews et al. 1987)

$$\frac{\partial \bar{u}}{\partial t} = \bar{v}^* \left[f - \frac{(\bar{u}\cos\phi)_\phi}{a\cos\phi} \right] - \bar{w}^* \bar{u}_z + \frac{\nabla \cdot \mathbf{F}}{a\cos\phi}, \qquad (1)$$

where a is the radius of the planet. (1) shows that the eddies contribute to both the mean zonal torque, $\partial\bar{u}/\partial t$, and to the residual velocities $(0, \bar{v}^*, \bar{w}^*)$. As seen from Figs. 1b, d, the areas of strong wave forcing coincide with the areas of enhanced meridional transport in the middle atmosphere. It was shown in Hartogh et al. (2005) that the former forces the latter to a large degree. The horizontally transported air descends in high winter latitudes. During dust storms and the associated increase of mechanical forcing, the subsiding motions intensify, in accordance with the "downward control" principle (Haynes et al. 1991).

This analysis illustrates the relation between the increased temperature over the winter pole during dust storms and the enhanced wave forcing in the middle atmosphere. To elucidate the role of different types of eddies in this process, we performed simulations with (i) a flat surface, and (ii) with the diurnal insolation cycle replaced by its mean value. Thus, generation of SPWs was inhibited in the former run, and tides were excluded in the latter. The results for the "strong dust" scenario are plotted in Fig. 2. The differences in the simulated temperature and that from the "full physics" run (Fig. 1c) are

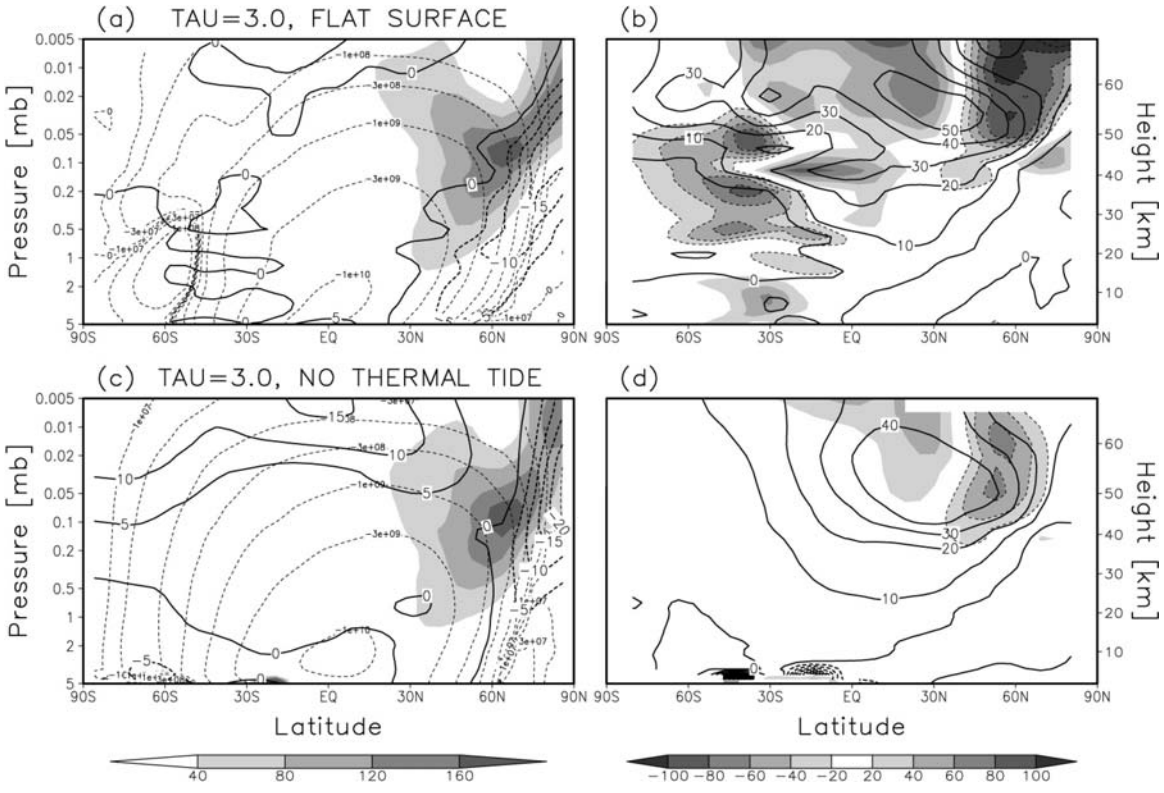

Fig. 2. Results of the simulations for the "strong dust" ($\tau = 3.0$) with the "flat surface" (upper panels) and "no tides" (lower panels): (a) and (c) Same as left panels in Fig. 1, except that the bold contours denote the difference of the simulated zonal-mean temperature with the "full physics" run in Fig. 1c; (b) and (d) same as right panels in Fig. 1.

denoted with bold contour lines in Figs. 2a, c. They show that the winter polar air becomes up to 20 K colder without SPWs, and up to 25 K colder without tides. Accordingly, the adiabatic heating rates shown by the shading are smaller than in Fig. 1c. This demonstrates that both SPWs and tides contribute to strengthening the polar warmings. Note that tides, unlike SPWs, are responsible also for up to 15 K cooling in the upper part of the model domain at all latitudes except above the North Pole. Figs. 2b, d present the corresponding $\bar{v}^*$ and $\nabla \cdot \mathbf{F}$ for the simulations with the flat surface and diurnal-mean insolation, respectively. It is seen that the elimination of SPWs slows down the meridional transport (the maximum of $\bar{v}^*$ decreases by ~ 10 m s^{-1}), while it does not affect the maximum of $\nabla \cdot \mathbf{F}$ above the northern subtropics. Meanwhile, the elimination of tides results in a dramatic reduction of the eddy forcing and the meridional velocity in the summer hemisphere, and in ~ 20 m s^{-1} slower $\bar{v}^*$ and ~ 40 m s^{-1} sol^{-1} weaker $\nabla \cdot \mathbf{F}$ in the winter hemisphere.

To evaluate the contribution of different waves to the eddy forcing of the meridional circulation further, we performed the temporal and spatial Fourier analysis of the 3-hourly model output, similar to the one described by Kuroda et al. (2008). Figure 3 displays the EP flux divergence and its spectral components calculated for the "dust storm" run including the full physics. The total $\nabla \cdot \mathbf{F}$ is shown in Fig. 3a, and the contribution of all tidal components (from diurnal to quad-diurnal

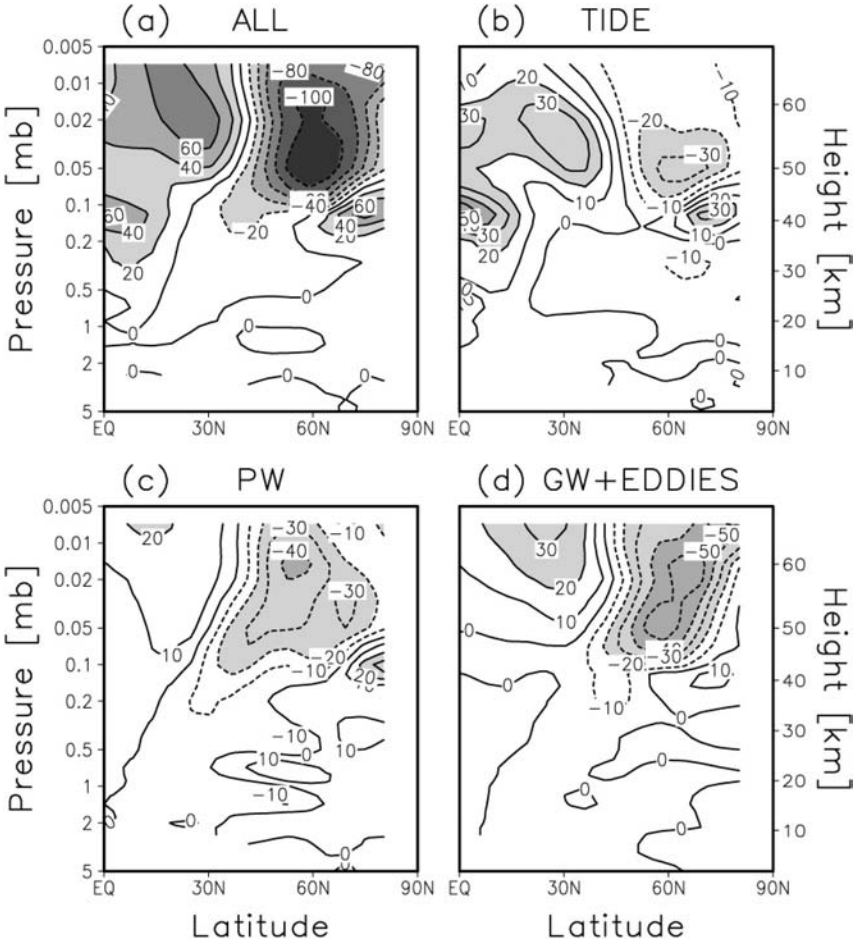

Fig. 3. EP flux divergence $\nabla \cdot \mathbf{F}$ [m s^{-1} sol^{-1}] for the "strong dust" ($\tau = 3.0$) "full physics" simulation: (a) The total $\nabla \cdot \mathbf{F}$; (b) contribution of tides (the sum of the diurnal to quad-diurnal components with $s = 1$ to 10); (c) contribution of planetary waves; (d) contribution of gravity waves and eddies (with $s > 10$ and periods less than a day).

for both westward and eastward propagating harmonics with zonal wavenumbers from $s = 1$ to 10, i.e., migrating and non-migrating tides) is plotted in Fig. 3b. The EP flux divergence associated with all planetary waves (the sum of eastward and westward propagating waves with periods greater than 1 sol) is given in Fig. 3c. Shorter-scale harmonics with periods of ≤ 1 sol except tides represent resolved gravity waves and eddies, and their contribution to $\nabla \cdot \mathbf{F}$ is shown in Fig. 3d. It is seen that tides, planetary and gravity waves and eddies provide an eastward momentum in low latitudes, and a westward momentum in mid- and high latitudes, except over the pole around 0.1 mb. These areas of positive and negative torque largely coincide with the mean zonal easterlies and westerlies, correspondingly. However, as follows from (1), the mean zonal flow tendency is affected not only by the non-zonal disturbances but also by the meridional circulation. The analysis of all terms in (1) shows that positive $\nabla \cdot \mathbf{F}$ in low and midlatitudes is compensated by the northward advection, and negative $\nabla \cdot \mathbf{F}$ in high latitudes is offset by the southwardly slanted air descent. It immediately stands out from Fig. 3 that the tides, planetary waves and smaller-scale gravity waves and eddies almost equally contribute to the total forcing. The role of gravity waves grows with height, which is likely related to the enhanced dissipation by the sponge layer near the model lid. Tidal forcing is strong in the equatorial area, and, what is less expected, in high winter latitudes. The eastward torque provided by the tides in low latitude ($< 30°$N) middle atmosphere is indicated also in another model simulation (Moudden and Forbes 2008). The EP fluxes for the migrating diurnal and semidiurnal tides are plotted with arrows in Figs. 4a, b, correspondingly. A strong divergence of both components occurs above the equator between 0.2 and 0.1 mb. It corresponds to the local maximum of $\nabla \cdot \mathbf{F} > 50$ m s^{-1} sol^{-1} in

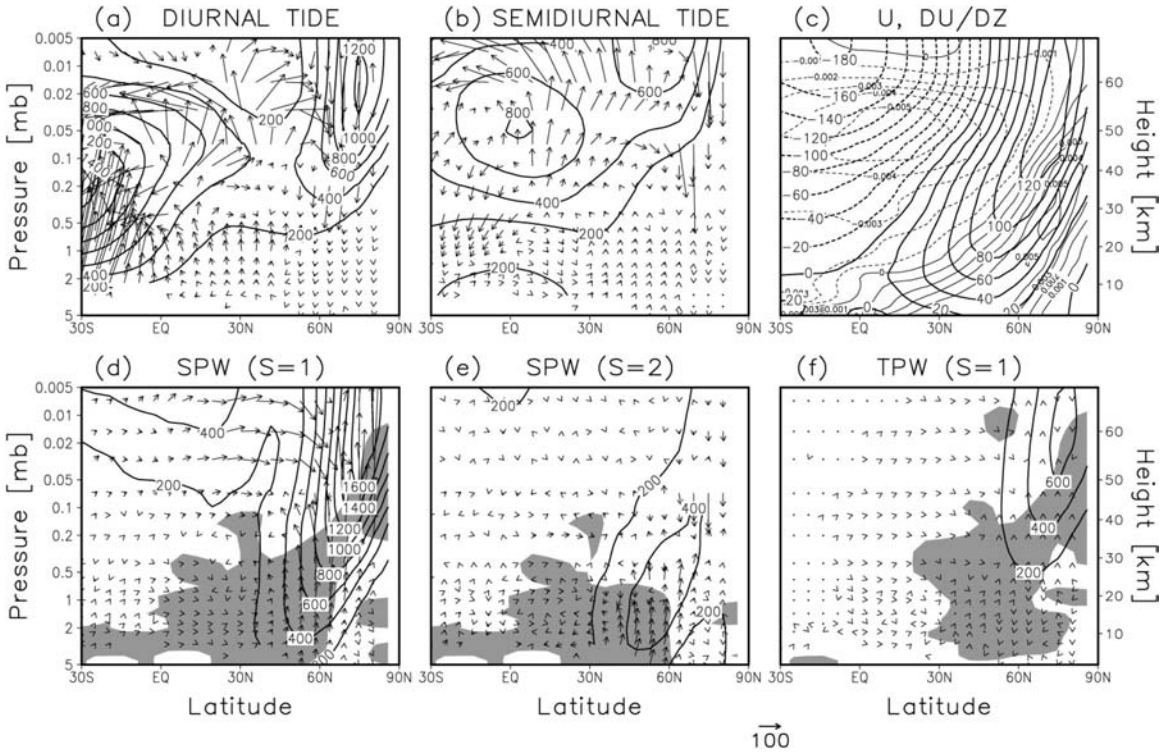

Fig. 4. Wave geopotential height amplitudes [m] (contour lines), the square of the refractive index (shaded in positive regions, only for planetary waves), and the EP fluxes [m^2 s^{-2}] (arrows, the scale of meridional fluxes is shown in the bottom of the figure and the vertical fluxes are multiplied by 125) for (a) diurnal tides, (b) semidiurnal tides, (d) SPW ($s = 1$), (e) SPW ($s = 2$), and (f) eastward propagating TPW with the period of 5.0 sols and $s = 1$. The panel (c) shows the mean zonal wind [m s^{-1}] (bold contour lines) and the vertical wind shear [s^{-1}] (thin lines).

Fig. 3b, and indicates an enhanced thermal excitation of tides (Fels and Lindzen 1974). The other area of strong EP flux divergence is located over 30°N at ~ 0.02 mb, where the vertical shear $\bar{u}_z < 0$ is large (Fig. 4c). As a result, the main contribution to $\nabla \cdot \mathbf{F}$ comes from the meridional gradient of $\mathbf{F}$ containing the southward heat flux. This example illustrates that tidal influences on the mean flow are more complex than simply a westward torque, especially in regions of their excitation and/or strong mean wind shear.

In our simulations, the main source of the diurnal tide lies in the summer southern hemisphere, in particular over the subsolar point at around 30°S (Fig. 4a). Semidiurnal tides are excited in the equatorial middle atmosphere (Fig. 4b). Increasing the dust loading (from $\tau = 0.5$ to 3.0) enhances the absorption of solar radiation by aerosol and the excitation of tides, which results in almost 3 times larger EP fluxes in the southern hemisphere. Further propagation of the tides to high winter latitudes is less affected by the changes in the mean zonal circulation. Consequently, the tidal amplitude and the corresponding EP flux divergence over the North Pole increased by a factor 3 in the dust storm simulation.

Among planetary waves contributing to the forcing in Fig. 3c, the most dominant are SPWs with zonal wavenumbers $s = 1$ and 2, and the eastward-propagating transient planetary wave (TPW) with $s = 1$ and 5 sols period. The amplitudes of the geopotential height as well as the corresponding squared refractive indices, n_s^2, for the three types of waves are shown in Figs. 4d, e and f. The index n_s^2 is calculated as follows:

$$n_s^2 = \frac{\bar{q}_y}{\bar{u} - c} - \frac{s^2}{a^2 \cos^2 \phi} - \frac{f^2}{4N^2H^2}, \qquad (2)$$

where $\bar{q}_y$ is the mean potential vorticity gradient, $\bar{u}$ is the zonal-mean zonal wind velocity, c is the phase speed of the wave, and N is the Brunt-Väisälä frequency. The shaded areas with $n_s^2 > 0$ denote regions of free vertical and meridional wave propagation. It is seen that the SPW ($s = 1$) dominates in the winter hemisphere during dust storms (Fig. 4d). Its amplitude increases almost tenfold compared to the $\tau = 0.5$ simulation. This chiefly occurs due to the weakening of the westerly jet during dust storms, which creates favorable conditions for vertical propagation. Additionally, the near surface westerlies flowing over topography extend farther into low latitudes in times of dust storms. Thus, SPWs are generated over larger territory. As a result, the EP fluxes associated with the SPW ($s = 1$) in the lower atmosphere are more than twice as large in our $\tau = 3.0$ run. Unlike the case for the $s = 1$ harmonic, the SPW ($s = 2$) is weaker, and is located lower (Fig. 4e). Its amplitude and the produced forcing vary little between the two runs, constitutes about one half of that by the SPW ($s = 1$) below 0.5 mb, and is negligible above 0.1 mb. Finally, the eastward-propagating TPW ($s = 1$) is generated in the upper atmosphere (Fig. 4f). The change of sign of $\bar{q}_y = \beta - f^2\rho^{-1}(\rho N^{-2}\bar{u}_z)_z - \bar{u}_{yy}$ in the model domain, where $\beta = df/dy$ and ρ is the atmospheric density, represents the necessary condition for instability (Andrews et al. 1987). In this simulation, $\bar{q}_y$ becomes negative in the low and midlatitudes above ~ 0.05 mb, and in high latitudes below ~ 0.5 mb. As seen in Fig. 4c, the former is due to large $\bar{u}_{yy} > 0$, and the latter is due to large $\bar{u}_{zz} > 0$. The instability in high latitude lower atmosphere is the source of baroclinic waves (Kuroda et al. 2007). Therefore, the TPWs are likely generated due to the barotropic instability in low latitudes, similar to the ~ 10-sol wave in Wilson et al. (2002), and due to baroclinic instability in high latitudes. Its amplitude and contribution to $\nabla \cdot \mathbf{F}$ above 0.1 mb increase by factor of ~ 2 in the dust storm simulation, which corresponds to about 1/3 of the forcing by the SPW ($s = 1$). Note that the generation of TPWs in the lower atmosphere is suppressed during dust storms due to the stabilization of the jet stream with respect to baroclinic disturbances (Kuroda et al. 2007).

4. Conclusions

A general circulation model of the Martian atmosphere was used to explore the changes in the meridional circulation that lead to temperature increases observed over winter poles during planet-encircling solstitial dust storms. In the absence of direct solar heating, these temperature vertical inversions have a dynamical origin, and are due to a strengthening of the overturning meridional circulation. While Wilson (1997) emphasized the dominant role of tides in extending the circulation further to the winter pole, we show that dissipating tides, planetary waves, resolved gravity waves and geostrophic eddies almost equally contribute to the forcing that causes warming in high-latitude winter middle atmosphere at times of high atmospheric aerosol content. The amplification of tidal amplitudes in the near-pole region (and of the associated

wave forcing of the poleward and downward flow aloft) is the direct result of stronger excitation of tides in the summer hemisphere, especially around the subsolar latitude. The other two thirds of forcing required for the intensification of the meridional circulation are delivered by planetary and resolved smaller-scale gravity waves and eddies. Among planetary waves, the stationary wave (SPW) with the zonal wavenumber $s = 1$ is a major contributor. Changes in the circulation caused by dust storms allow for stronger generation of this wave in the lower atmosphere (due to the equatorward extension of near-surface westerlies), and, what is more important, for its more favorable vertical propagation. SPW ($s = 2$) is less affected by dust storms, dissipates lower, and contributes to the adiabatic heating mainly below 0.1 mb. Above this height a transient planetary wave with a barotropic/baroclinic vertical structure ($s = 1$ and period ~ 5 sols, in our simulations) also provides a momentum that represents about 1/3 of that of the SPW ($s = 1$). Finally, our results indicate for the first time the importance of resolved gravity waves and eddies in maintaining the meridional circulation in the Martian middle atmosphere, at least in high winter latitudes during dust storms. In spite of the relatively coarse horizontal resolution, the contribution of resolved, small-scale gravity waves to the total eddy forcing is approximately equal to that of tides and planetary waves. We speculate that the gravity wave contribution may increase when additional waves are resolved.

Acknowledgements

This work was partially supported by German Research Foundation (DFG), grant HA 3261/3, and the Research Fellowships of the Japan Society for the Promotion of Science (JSPS) for Young Scientists, Grant-in-Aid 20·1761. Comments of John Wilson of GFDL and an anonymous reviewer helped to improve the presentation.

References

Andrews, D. G., and M. E. McIntyre, 1976: Planetary waves in horizontal and vertical shear: The generalized Eliassen-Palm relation and the mean zonal acceleration. *J. Atmos. Sci.*, **33**, 2031–2048.

Andrews, D. G., J. R. Holton, and C. B. Leovy, 1987: *Middle Atmosphere Dynamics*, International Geophysics Series. Vol. 40, Academic Press, Orlando, 489 pp.

Barnes, J. R., and R. M. Haberle, 1996: The Martian zonal-mean circulation: Angular momentum and potential vorticity structure in GCM simulations. *J. Atmos. Sci.*, **53**, 3143–3156.

Barnes, J. R., and J. L. Hollingsworth, 1987: Dynamical modeling of a planetary wave mechanism for a Martian polar warming. *Icarus*, **71**, 313–334.

Bougher, S. W., J. M. Bell, J. R. Murphy, M. A. Lopez-Valverde, and P. G. Withers, 2006: Polar warming in the Mars thermosphere: Seasonal variations owing to changing insolation and dust distributions. *Geophys. Res. Lett.*, **33**, L02203, doi:10.1029/2005GL024059.

Deming, D., M. J. Mumma, F. Espenal, T. Kostiuk, and D. Zipoy, 1986: Polar warmings in the middle atmosphere of Mars. *Icarus*, **66**, 366–379.

Fels, S. B., and R. S. Lindzen, 1974: The interaction of thermally excited gravity waves with mean flows. *Geophys. Fluid. Dyn*, **6**, 149–191.

Forget, F., F. Hourdin, R. Fournier, C. Hourdine, O. Talagrand, M. Collins, S. R. Lewis, P. L. Read, and J. -P. Huot, 1999: Improved general circulation models of the Martian atmosphere from the surface to above 80 km. *J. Geophys. Res.*, **104**, 24155–24175.

Hartogh, P., A. S. Medvedev, T. Kuroda, R. Saito, G. Villanueva, A. G. Feofolov, A. A. Kutepov, and U. Berger, 2005: Description and climatology of a new general circulation model of the Martian atmosphere. *J. Geophys. Res.*, **110**, E11008, doi:10.1029/2005JE002498.

Haynes, P. H., C. J. Marks, M. E. McIntyre, T. G. Shepherd, and K. P. Shine, 1991: On the "downward control" of extratropical diabatic circulations by eddy-induced mean zonal forces. *J. Atmos. Sci.*, **48**, 651–678.

Jakosky, B. M., and T. Z. Martin, 1987: North-polar atmospheric temperatures during dust storms. *Icarus*, **72**, 528–534.

Keating, G. M., M. Theriot, R. Tolson, S. Bougher, F. Forget, and J. Forbes, 2003: Brief review on the results obtained with the MGS and Mars Odyssey 2001 Accelerometer Experiments. in *International Workshop on Mars Atmosphere Modeling and Observations*, edited by F. Forget et al., LMD, IAA, AOPP, CNES and ESA, Granada, Spain, 2 pp.

Kuroda, T., N. Hashimoto, D. Sakai, and M. Takahashi, 2005: Simulation of the Martian atmosphere using a CCSR/NIES AGCM. *J. Meteor. Soc. Japan*, **83**, 1–19.

Kuroda, T., A. S. Medvedev, P. Hartogh, and M. Takahashi, 2007: Seasonal change of the baroclinic wave activity in the northern hemisphere of Mars simulated with a GCM. *Geophys. Res. Lett.*, **34**, L09203, doi:10.1029/2006GL028816.

Kuroda, T., A. S. Medvedev, P. Hartogh, and M. Takahashi, 2008: Semiannual oscillations in the atmosphere of Mars. *Geophys. Res. Lett.*, **35**, L23202, doi:10.1029/2008GL036061.

McCleese, D. J., et al., 2008: Intense polar temperature inversion in the middle atmosphere of Mars. *Nature Geoscience*, **1**, 745–749.

Medvedev, A. S., and P. Hartogh, 2007: Winter polar warmings and the meridional transport on Mars simulated with a general circulation model. *Icarus*, **186**, 97–110.

Moudden, Y., and J. M. Forbes, 2008: Effects of vertically propagating thermal tides on the mean structure and dynamics of Mars' lower thermosphere. *Geophys. Res. Lett.*, **35**, L23805, doi:10.1029/2008GL036086.

Numaguti, A., M. Takahashi, T. Nakajima, and A. Sumi, 1995: Development of atmospheric general circulation model. *Climate System Dynamics and Modeling*, edited by T. Matsuno, Center for Climate System Research, University of Tokyo, Tokyo, 1–27.

Schneider, E. K., 1977: Axially symmetric steady-state models of the basic state for instability and climate studies. Part II. Non-linear calculations. *J. Atmos. Sci.*, **34**, 280–296.

Schneider, E. K., 1983: Martian great dust storms: Interpretive axially symmetric models. *Icarus*, **55**, 302–331.

Smith, M. D., 2004: Interannual variability in TES atmospheric observations of Mars during 1999–2003. *Icarus*, **167**, 148–165.

Theodore, B., E. Lellouch, E. Chassefiere, and A. Hauchecorne, 1993: Solstitial temperature inversions in the martian middle atmosphere: Observational clues and 2-D modeling. *Icarus*, **105**, 512–528.

Wilson, R. J., and K. Hamilton, 1996: Comprehensive model simulation of thermal tides in the Martian atmosphere. *J. Atmos. Sci.*, **53**, 1290–1326.

Wilson, R. J., 1997: A general circulation model of the Martian polar warming. *Geophys. Res. Lett.*, **24**, 123–126.

Wilson, R. J., D. Banfield, B. J. Conrath, and M. D. Smith, 2002: Traveling waves in the Northern Hemisphere of Mars. *Geophys. Res. Lett.*, **29**, doi:10.1029/2002GL014866.

Yamashita, Y., T. Kuroda, and M. Takahashi, 2007: Maintenance of zonal wind variability associated with the annular mode on Mars. *Geophys. Res. Lett.*, **34**, L16819, doi:10.1029/2007GL030069.